Available online at www.sciencedirect.com
SCIENCE DIRECT
Journal of Catalysis 231 (2005) 115–130
JOURNAL OF CATALYSIS
www.elsevier.com/locate/jcat

Selective oxidation of methane over MoO_x/SiO_2: isolation of the kinetics of reactions occurring in the gas phase and on the surfaces of SiO_2 and MoO_x

Nicholas Ohler, Alexis T. Bell *

Department of Chemical Engineering, University of California, Berkeley, CA 94720-1462, USA

Received 7 August 2004; revised 17 December 2004; accepted 20 December 2004

Abstract

The selective oxidation of methane to formaldehyde over MoO_x/SiO_2 was investigated to identify the contributions of methane and formaldehyde reactions occurring in the gas phase and on the surfaces of SiO_2 and dispersed MoO_x to the overall observed reaction rate. Experiments were conducted with 4.5 wt% MoO_3/SiO_2 at a nominal surface concentration of 0.44 Mo nm^{-2}. Data were acquired for CH_4/O_2 ratios from 2 to 34 and temperatures from 848 to 923 K. Homogeneous oxidation of methane was negligible, and the homogeneous oxidation of formaldehyde contributed only to a small degree. The formation of formaldehyde was found to occur largely over MoO_x and only to a limited degree over SiO_2. By contrast, the rates of formaldehyde consumption over MoO_x and SiO_2 were comparable. For SiO_2 the only process occurring was CH_2O decomposition, which was independent of the CH_4/O_2 ratio, whereas in the case of MoO_x, CH_2O decomposition was accompanied by combustion of the H_2 formed and by direct CH_2O combustion principally to CO. A comprehensive model of the overall reaction kinetics was assembled from the kinetics determined for the reactions of methane and formaldehyde in the gas phase and on the surfaces of SiO_2 and MoO_x. This model describes the observed rates of methane conversion and the formaldehyde selectivity measured experimentally as functions of temperature and CH_4/O_2 ratio. This model is then used to determine the maximum single-pass yield of CH_2O for a given temperature and CH_4/O_2 ratio. It is predicted that the maximum single-pass yield increases with reaction temperature and decreasing CH_4/O_2 ratio.

Keywords: Methane; Formaldehyde; Methane oxidation; Formaldehyde oxidation; MoO_3/SiO_2; Molybdena; Silica

1. Introduction

The selective oxidation of methane to formaldehyde in a single step is a challenging problem of great practical importance [1]. Silica-supported oxides are among the best-performing heterogeneous catalysts for the selective oxidation of methane, especially the supported oxides of Mo, V, and Fe [2–4]. Silica has emerged as the preferred support because other refractory supports, such as TiO_2 and Al_2O_3, burn formaldehyde very rapidly at temperatures well below those required for the activation of methane [5]. Although SiO_2 is inert to CH_2O relative to other supports, it still decomposes CH_2O rapidly at temperatures and contact times relevant to methane oxidation [6]. Since the optimum metal loading needed to achieve maximum formaldehyde yield is well below monolayer coverage [2,7], most of the exposed surface area is SiO_2. The loss of CH_2O via homogeneous reaction is also known to occur [8,9] and has been implicated as a primary factor limiting CH_2O yield during CH_4 oxidation over MoO_x/SiO_2 [7]. However, previous studies modeling the kinetics of CH_4 oxidation over bare SiO_2 and MoO_x/SiO_2 have ignored the gas-phase contribution to the CH_2O reaction rate [10–13]. Therefore the question arises, how much of a role do the silica support and the gas phase play in determining the product distribution during methane oxidation over silica-supported oxides?

* Corresponding author.
E-mail address: bell@cchem.berkeley.edu (A.T. Bell).

0021-9517/$ – see front matter
doi:10.1016/j.jcat.2004.12.024

The selective oxidation of methane to formaldehyde may be reduced to two processes, the formation and consumption of the product formaldehyde. The kinetics of formaldehyde consumption (i.e., decomposition and oxidation) have typically been studied indirectly by analysis of rate data for methane oxidation. However, we can obtain a better understanding of the kinetics of CH_2O decomposition and oxidation by studying these secondary processes independently of CH_4 oxidation.

This study focuses on decoupling the rates of reaction occurring over MoO_x/SiO_2. The rates of CH_4 oxidation and CH_2O consumption occurring in the gas phase, on the SiO_2 support, and on the MoO_x sites are decoupled through kinetic analysis of CH_4 oxidation and CH_2O reaction data obtained over a wide range of feed compositions and over a range of temperatures relevant to methane activation (> 848 K). The reaction network and rate laws utilized are justified by kinetic analysis. The individually measured kinetics are assembled to describe the relevant processes occurring during CH_4 oxidation over MoO_x/SiO_2. The model is used to describe the effects of operating conditions on catalyst performance and to define the contributions of the gas phase, exposed support, and supported MoO_x to the overall rates of methane oxidation and formaldehyde consumption.

2. Experimental

A MoO_x/SiO_2 catalyst was prepared by aqueous impregnation of Silicycle 60-Å silica gel with ammonium heptamolybdate (AHM) tetrahydrate (Aldrich 99.98% pure). The bare silica gel was washed in 9 M HNO_3 at 333 K, rinsed thoroughly with deionized water, and calcined in flowing air for 3 h at 973 K to remove alkaline earth impurities [14,15]. This treatment reduced the silica surface area from 500 to 460 $m^2\,g^{-1}$, as measured by five-point BET analysis of N_2 adsorption isotherms. AHM (0.067 g) was dissolved in 2.1 g of deionized water (150% of the pore-filling amount) for each gram of silica gel to be prepared. The silica and solution were mixed to dryness in a bath heated at 333 K, oven-dried at 383 K overnight, and calcined under flowing air at 873 K for 3 h before use. After loading with molybdena, the catalyst surface area was 426 $m^2\,g^{-1}$. Elemental analysis (Galbraith Laboratories) determined the Mo weight fraction to be 3.0% (4.5 wt% as MoO_3), so that the nominal surface coverage of MoO_x was 0.44 Mo nm^{-2}. The diameter of the catalyst particles was 200–500 μm, which was sufficiently small to ensure that the reactions were not limited by mass transfer according to the Weisz–Prater criterion [16]. The catalyst was used without adjustment of the size distribution or dilution.

The catalyst properties are summarized in Table 1. The parameter ζ describes the ratio of the exposed SiO_2 area per unit bed volume of the MoO_x/SiO_2 catalyst to that of the bare SiO_2, and is calculated as

$$\zeta = \frac{a_m \rho_b}{a_m^0 \rho_b^0}\left(1 - \frac{c_m}{c_m^{mono}}\right), \tag{1}$$

where a_m and ρ_b are the specific surface area and bulk density of the MoO_x/SiO_2 catalyst, respectively, and a_m^0 and ρ_b^0 are the corresponding parameters for the bare SiO_2. The term in parentheses accounts for the fraction of the surface of MoO_x/SiO_2 occupied by MoO_x. c_m is the surface concentration of Mo, and c_m^{mono} is the theoretical monolayer coverage of MoO_x, taken as 8.2 Mo nm^{-2} [17]. The porosity ε is calculated from the bulk density ρ_b and skeletal density ρ_s of each catalyst as

$$\varepsilon = \frac{\rho_b}{\rho_\varepsilon} = 1 - \frac{\rho_b}{\rho_s}, \tag{2}$$

where ρ_b was measured by volumetry, and ρ_s was estimated from linear summation of skeletal densities of the SiO_2 and MoO_x, assuming the MoO_x to be present as bulk MoO_3:

$$\rho_s = (2.20\ \mathrm{g\,cm^{-3}})(1 - \omega_{MoO_3}) + (4.62\ \mathrm{g\,cm^{-3}})\omega_{MoO_3}, \tag{3}$$

where ω_{MoO_3} is the weight fraction of MoO_x as MoO_3.

Raman spectra were recorded with a Kaiser Optical HoloLab 5000 series Raman spectrometer equipped with a Nd:YAG laser that was frequency-doubled to 532 nm and operated at 7 mW. Catalyst samples (50–100 mg) were ground into powder and pressed into discs 1 cm in diameter at 10,000 psi. The discs were placed in a sealed rotary cell and rotated at 400 rpm during laser exposure to distribute the beam over a greater area and reduce local heating. The cell was heated to 923 K with air flowing over the samples to examine the state of the catalysts at a temperature relevant to CH_4 oxidation. Cubic splines were utilized to remove background fluorescence. Raman peak positions were reproducible to within 1 cm^{-1} for strong peaks and 2 cm^{-1} for all peaks.

Flow experiments were conducted by supporting the catalyst on a plug of quartz wool in a quartz reactor with a quartz-sheathed thermocouple inserted halfway into the bed

Table 1
Catalyst physical properties

Catalyst	Mo surface concentration c_{Mo} (Mo nm^{-2})	Specific surface area a_m ($m^2\,g^{-1}$)	Bulk density ρ_b ($g\,cm^{-3}$)	Skeletal density ρ_s ($g\,cm^{-3}$)	Porosity ε	Residual exposed surface area ζ
SiO_2	–	460	0.570	2.20	0.741	1
MoO_x/SiO_2	0.44	426	0.660	2.28	0.711	1.01

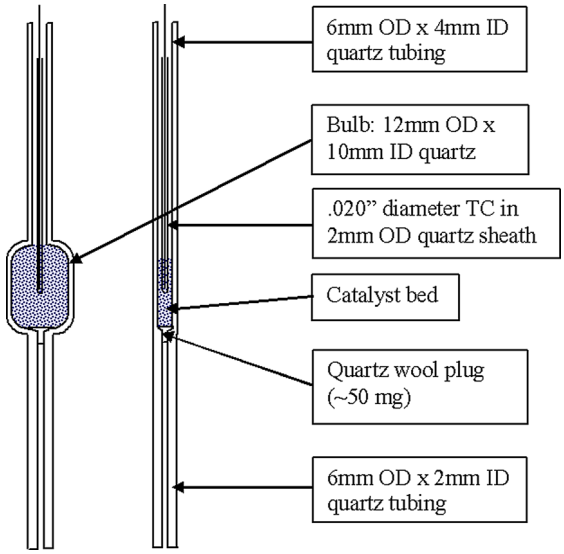

Fig. 1. Schematic of reactor configurations utilized. The bulbless configuration was used for most of the experiments. The configuration utilizing a bulb was utilized to gather data at long contact times.

for temperature control. Two reactor geometries were utilized: one with a bulb and one without, depending on how much catalyst was needed. The reactors are shown schematically in Fig. 1. The tubing downstream of the bulb was of smaller diameter (2 mm) so that the product gases would be transported out of the heated zone as rapidly as possible after they left the catalyst bed [7]. The mass of the quartz wool plug was approximately 50 mg. We measured the activity of the quartz wool plug by running the reactor with and without the plug in place. The activity of the plug was undetectable for CH_4 oxidation and reacted with less than 5% of the CH_2O fed under the slowest flow conditions employed here.

The reactor was heated over a 15-cm zone with a 60-V Omegalux radiant heater (Omega CFRC-16/60-C-A). The vestibules at each end of the heater were stuffed with glass wool insulation. CH_4, O_2, and He were delivered to the manifold via Porter 201 mass flow controllers, which were calibrated with a bubble meter. CH_2O was added to the feed stream by passing on O_2/He flow through a saturator filled with beads of solid paraformaldehyde (Aldrich; 95% pure). We controlled the CH_2O vapor pressure in the saturator by recirculating heated water through a jacket surrounding the saturator. The temperature of the water was controlled with a Thermo Electron Neslab RTE-7 recirculating heater/chiller. A temperature of about 331 K was necessary to achieve a vapor pressure of 0.01 atm CH_2O in the saturator. Typical formaldehyde molar fractions observed during CH_4 oxidation were on the order of 1%, so similar molar fractions were targeted for studies of formaldehyde consumption. The feed flow could be directed through the catalyst bed or through a bypass for analysis of feed composition. All tubing downstream of the saturator was maintained at about 423 K with heat tapes to prevent condensation of water or solid paraformaldehyde on the tubing walls. Pressure was monitored with a pressure transducer (Omega PX 543-150GI) positioned before the reactor. A National Instruments LabView interface was utilized with a Porter PCIM-4 controller to apply composition and total flow program setpoints to the mass flow controllers, and with an Omega CN3251 controller to apply temperature program setpoints to the radiant heater. Contact times were determined taking total pressure and temperature, as well as molar flow rates, into account, since the pressure was as high as ~ 2 atm for the highest flow rates utilized:

$$\tau = \frac{V}{F'} = \left(\frac{m\varepsilon}{\rho_b}\right) \Big/ \left(\frac{FRT}{P}\right). \tag{4}$$

In this expression, τ is the contact time, V is the gas volume within the catalyst bed, F' is the volumetric flow rate, m is the catalyst mass, ε is the catalyst porosity, ρ_b is the bulk catalyst density, F is the molar flow rate, R is the gas constant, T is the absolute temperature, and P is the total pressure. This definition differs slightly from the definition of space time, in which the reactor volume is the total volume occupied by the catalyst bed (the factor ε is omitted). The contact time defined in this way accurately reflects the amount of time the gas is within the catalyst bed. This detail becomes important when analysing homogeneous rates of reaction within a catalyst bed.

An HP 6890N gas chromatograph with a heated 250-µl sampling loop was used to measure the composition of both the reactor feed and the reactor effluent. A 30-foot-long, 1/8-inch-diameter column packed with Hayesep DB 80/100 mesh was used to separate all components. The column temperature was held at 278 K for 7 min, ramped at 45 K min^{-1} to 423 K, and held at 423 K for 15 min. Eluted components were detected with a thermal conductivity detector. Repeated measurements of feed flows demonstrated standard deviations of 2% or less for all feed components relative to mean amounts. CH_2O peak areas were calibrated in the following manner. A mixture of CH_2O, O_2, and He was passed through reactor loaded with 5% Pd/Al_2O_3, which combusted CH_2O completely to CO_2. The amount of CH_2O responsible for each CH_2O peak observed during bypass of the reactor was set equal to the corresponding amount of CO_2 observed after complete combustion.

3. Modeling methods

During CH_4 oxidation over MoO_x/SiO_2, reactions can occur in the gas phase, on the exposed SiO_2 support, and on the supported MoO_x. To ascertain the contributions of each of these reactive media to the observed reaction rates, reactions were conducted with an empty reactor and with the reactor filled with either bare SiO_2 or the MoO_x/SiO_2 catalyst. The overall (observed) rate of reaction is assumed to be the sum of the individual contributions. For reactions over bare SiO_2, the observed reaction rates are assumed to include the

rates in the gas phase and the rates on the SiO_2 surface. For reactions over MoO_x/SiO_2, the rates include both of these contributions and the contribution of the supported MoO_x moieties. Denoting homogeneous reaction with H, reaction on the SiO_2 surface with S, and reaction on the supported MoO_x with M, the observed rates over SiO_2 are thus

$$r_i = \varepsilon r_{i\mathrm{H}} + r_{i\mathrm{S}} \tag{5}$$

and the rates over MoO_x/SiO_2 are

$$r_i = \varepsilon r_{i\mathrm{H}} + \zeta r_{i\mathrm{S}} + r_{i\mathrm{M}}. \tag{6}$$

In Eqs. (5) and (6), all rates have units of mol $\mathrm{cm}^{-3}\,\mathrm{s}^{-1}$. Surface reaction rates are normalized by catalyst bed volume to allow summation with the homogeneous reaction rate. The rates are easily converted to the typical area or molar bases by multiplication by the appropriate bulk catalyst properties taken from Table 1:

$$r'_{i\mathrm{S}}\ (\mathrm{mol}_i\,\mathrm{m}^{-2}\,\mathrm{s}^{-1}) = \frac{r_{i\mathrm{S}}\ (\mathrm{mol}_i\,\mathrm{cm}^{-3}\,\mathrm{s}^{-1})}{a^0_{\mathrm{m}}\ (\mathrm{m}^2\,\mathrm{g}^{-1}) \times \rho^0_{\mathrm{b}}\ (\mathrm{g}\,\mathrm{cm}^{-3})}, \tag{7}$$

$$\begin{aligned} r''_{i\mathrm{M}}\ &(\mathrm{mol}_i\,\mathrm{mol}^{-1}_{\mathrm{Mo}}\,\mathrm{s}^{-1}) \\ &= \big(r_{i\mathrm{M}}\ (\mathrm{mol}_i\,\mathrm{cm}^{-3}\,\mathrm{s}^{-1}) \times 6.02 \times 10^{23}\ (\mathrm{Mo}\,\mathrm{mol}^{-1}_{\mathrm{Mo}})\big) \\ &\quad /\big(a_{\mathrm{m}}\ (\mathrm{m}^2\,\mathrm{g}^{-1}) \times \rho_{\mathrm{b}}\ (\mathrm{g}\,\mathrm{cm}^{-3}) \\ &\quad \times 10^{18}\ (\mathrm{nm}^2\,\mathrm{m}^{-2}) \times c_{\mathrm{Mo}}\ (\mathrm{Mo}\,\mathrm{nm}^{-2})\big). \end{aligned} \tag{8}$$

In Eqs. (5) and (6) the rate of homogeneous reaction $r_{i\mathrm{H}}$ is reduced by the factor ε to account for the fraction of the catalyst bed occupied by the gas phase. The rate of reaction over SiO_2 is assumed to be proportional to the SiO_2 surface area, and hence the rate of reaction over bare SiO_2 is multiplied by ζ in Eq. (6) in order to describe the extent to which such reaction contributes to the overall surface reaction occurring on MoO_x/SiO_2.

Reaction modeling and data fitting were performed with the use of a plug-flow reactor (PFR) model implemented in Mathematica. The effects of axial dispersion were examined but were found to have very little impact on the values of the extracted kinetic parameters, so an ideal PFR model was utilized. The differential equations describing the concentration profiles of gaseous and surface species were solved along the length of the reactor, with the NDSolve algorithm as a shooting method. The calculated gas-phase composition of the reactor effluent was compared with the experimentally observed effluent composition in terms of the mean observed reaction rate, calculated as

$$\langle r_i \rangle = \frac{F z_i X_i}{V} = \frac{F(z_i - y_i)}{V}, \tag{9}$$

where X_i, y_i, and z_i are, respectively, the conversion, effluent fraction, and feed fraction of component i. For homogeneous reaction, V is the reactor volume. For reaction over a solid catalyst, V is the volume of the catalyst bed, m/ρ_{b}. Rates reported here are mean rates calculated according to Eq. (9) unless otherwise noted. We minimized the sum of the squared differences between the mean rates observed experimentally and calculated from the model by adjusting kinetic parameters with the FindMinimum search algorithm.

During CH_4 oxidation, O_2 was the limiting reagent. The O_2 conversion varied from 1% to as high as 95%, depending on operating conditions. During CH_2O oxidation/decomposition, CH_2O was the limiting reagent, and CH_2O conversions approached $\sim$ 75% in some cases. Because a plug-flow reactor model was used, and because the state of the surface is taken into account in the model, high reactant conversions do not present a problem in the analysis of the rate data.

4. Results and discussion

4.1. Catalyst characterization

The Raman spectra of the bare SiO_2 support under ambient conditions and at 923 K under flowing air are shown in Fig. 2. The spectra show features characteristic of the tetrahedral SiO_2 network at 430, 805, 1060, and 1180 cm^{-1}. The bands at 605 and 490 cm^{-1} are assigned to the D_1 and D_2 defect features, respectively, and the band at 970 cm^{-1} is assigned to the Si–O stretching vibrations of silanol groups [18–20]. The spectrum of the bare SiO_2 does not change upon heating to 923 K in flowing air, but the Raman scattering amplitude increases by about tenfold.

Raman spectra for the MoO_x/SiO_2 catalyst at ambient temperature and at 923 K are shown in Fig. 3. Under ambient conditions, the spectrum shows features at 870 and 955 cm^{-1} that are indicative of surface polymolybdate species [21,22]. Upon heating in dry flowing air to 923 K, the polymolybdate species disperse to yield isolated monooxo molybdate species, characterized by the single Mo=O

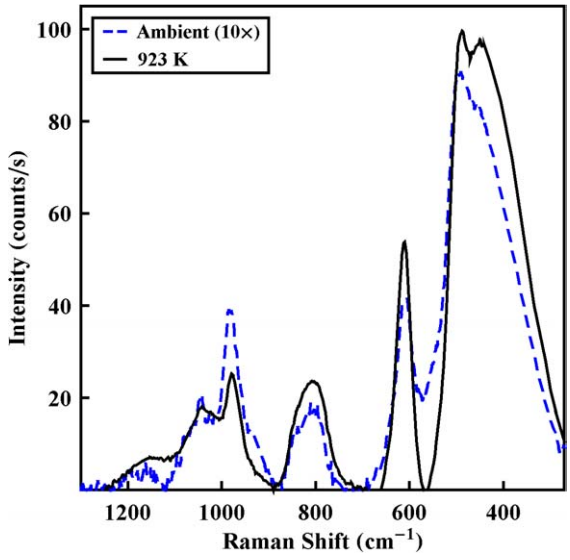

Fig. 2. Raman spectra of bare SiO_2 (a) under ambient conditions and (b) at 923 K under flowing air. Ambient spectrum amplified 10×.

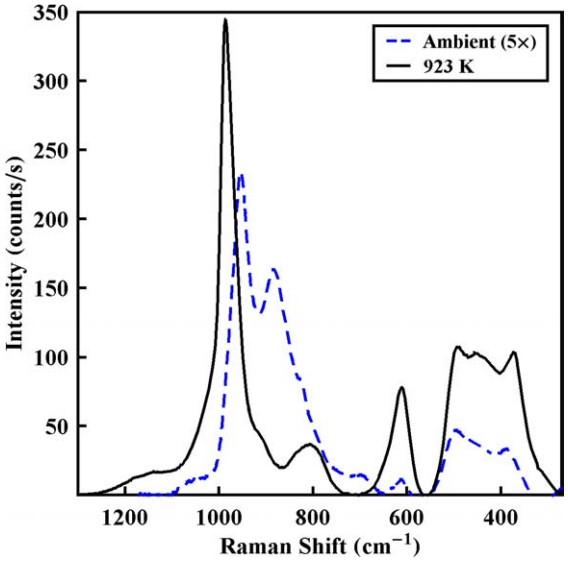

Fig. 3. Raman spectra of MoO_x/SiO_2 (a) under ambient conditions and (b) at 923 K under flowing air. Ambient spectrum amplified 5×.

stretching frequency observed at 985 cm^{-1} [22–28]. The SiO_2 features at 430, 490, 605, 805, and 1190 cm^{-1} are all clearly observed, but the features at 975 and 1060 cm^{-1} are obscured by the intense Mo=O stretching band. The feature at 370 cm^{-1} in the spectra of the MoO_x/SiO_2 under ambient conditions and at 923 K has been assigned as the bending mode of surface molybdate species [22]. The spectra observed under ambient conditions and during heating at 923 K are similar to those previously observed for MoO_x/SiO_2 prepared by deposition-precipitation [23]. The similarity of the Raman spectra is consistent with previous findings that the structure of SiO_2-supported MoO_x moieties is independent of the Mo precursor after high-temperature calcination [21]. Raman spectra similar to that shown in Fig. 3 have been recorded during CH_4 oxidation at 823 K [22,24,25], suggesting that supported MoO_x does not restructure under conditions of CH_4 oxidation.

The coordination of MoO_x/SiO_2 at these low weight loadings is octahedral under ambient conditions [21], but the structure under dehydrated conditions has been disputed in the literature, with some authors claiming tetrahedral coordination [26,27], others claiming distorted octahedral coordination [24,25,29,30], and some claiming a geometry "intermediate" between tetrahedral and octahedral [31]. The broad bands observed by UV–visible spectroscopy for this catalyst and the close proximity of the ligand-to-metal charge transfer bands for the T_d and O_h coordination preclude the use of the technique as a definitive indicator of coordination [29,32]. The most useful method for determining Mo coordination in this case is XANES. L_{III}-edge XANES data for MoO_x/SiO_2 suggest a degree of non-centrosymmetry for Mo intermediate between O_h and T_d [31]. Based on this observation and the observation by Raman and IR that the MoO_x/SiO_2 has a single terminal oxo group, it seems likely that the SiO_2-supported MoO_x moieties observed at 923 K

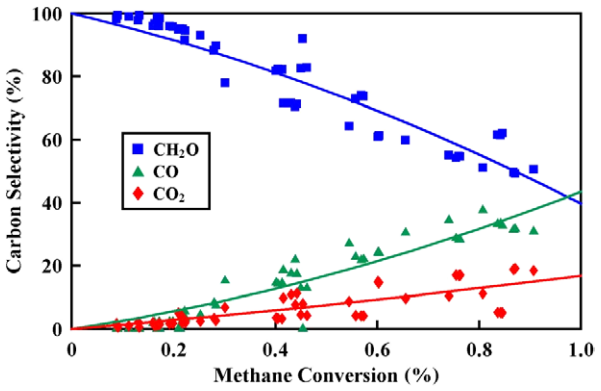

Fig. 4. Carbon selectivity versus methane conversion for methane oxidation over bare SiO_2 at 873 K. Feed composition is 90% CH_4, 10% O_2. CH_4 conversion was varied by varying contact time. Trendlines are empirical polynomial fits.

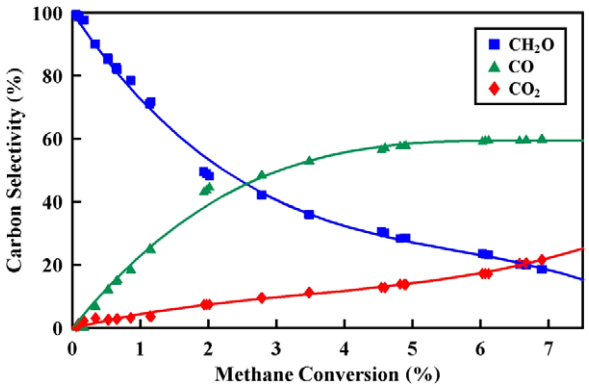

Fig. 5. Carbon selectivity versus methane conversion for methane oxidation over 0.44 Mo nm^{-2} MoO_x/SiO_2 at 873 K. Feed composition is 90% CH_4, 10% O_2. CH_4 conversion was varied by varying contact time. Trendlines are empirical polynomial fits.

are pentacoordinate. A trigonal bipyramid or square pyramid will have a degree of non-centrosymmetry intermediate between O_h and T_d and will have six total bonds with a single terminal oxo group. Such a coordination has previously been assigned to MoO_x/ZrO_2 at low loadings after calcination at 973 K, based on Raman spectroscopic observations [33].

4.2. Product distribution

The product distributions observed during CH_4 oxidation at 873 K over bare SiO_2 and over MoO_x/SiO_2 are plotted versus CH_4 conversion in Figs. 4 and 5, respectively. Over both catalysts the product distribution approaches 100% CH_2O as the CH_4 conversion approaches zero, demonstrating that CH_2O is the only initial product. As the CH_4 conversion increases, the CH_2O selectivity decreases and the selectivities for CO and CO_2 increase. These results demonstrate that CO_x is produced in secondary reactions from CH_2O.

Whereas several authors have also made observations indicating that the initial product distribution of CH_4 oxidation over MoO_x/SiO_2 is > 95% CH_2O [7,34–36], Spencer and Pereira reported a product distribution of 89% CH_2O and

11% CO_2 in the limit of zero CH_4 conversion [37]. A possible explanation for this discrepancy is the presence of CO_2 in the CH_4 supply. At very low CH_4 conversion, the concentration of CO_2 contaminant becomes comparable to the concentrations of reaction products, and the apparent initial product distribution will include this contaminant CO_2 if it is uncorrected.

Based on our observations of the change in product distribution with CH_4 conversion, we assume that CH_4 is oxidized selectively to CH_2O, and that CO_x (CO and CO_2) is formed solely from subsequent reaction of CH_2O:

$$CH_4 \rightarrow CH_2O \rightarrow CO_x.$$

Exclusion of a direct pathway from CH_4 to CO_2 allows CO and CO_2 to be treated as a single product (CO_x) in the analysis of the kinetics of CH_2O formation and consumption.

The ratio of CO/CO_2 observed during CH_2O oxidation/decomposition was about 12 over bare SiO_2 and about 9 over MoO_x/SiO_2. During CH_4 oxidation, the ratio was in the range of 8–10 over bare SiO_2 and 5.5–7 over MoO_x/SiO_2. The lower ratios observed during CH_4 oxidation are probably due to the higher partial pressure of H_2O during CH_4 oxidation and the water–gas shift equilibrium reaction, which lies toward CO_2 under the operating conditions employed in this study. Since the interconversion of CO and CO_2 was not investigated, no attempt was made to include the effects of this process in the modeling of CH_2O formation and consumption.

4.3. Methane oxidation

Homogeneous oxidation of CH_4 is not measurable under the conditions employed in this study. Whereas Baldwin et al. have found that homogeneous oxidation of CH_4 by O_2 becomes measurable at 923 K for residence times greater than 2 s and pressures greater than 2 atm [9], the contact times employed for CH_4 oxidation over MoO_x/SiO_2 are typically less than 1 s, and the pressures are typically less than 2 atm. Therefore only the contributions of the bare SiO_2 and supported MoO_x are considered in the modeling of CH_4 oxidation.

The kinetics of CH_4 oxidation over bare SiO_2 have been successfully described by Arena et al. with the use of a two-site, dissociative mechanism allowing for surface oxygen vacancies [10]. The model successfully described the extent of catalyst reduction observed by pulse O_2 chemisorption. The two-site dissociative mechanism includes the following reactions:

$$CH_4 + 2MO \rightarrow CH_2O + H_2O + 2M, \tag{1S}$$

$$CH_2O + \left(\frac{S_{CO} + 2S_{CO_2}}{S_{CO} + S_{CO_2}}\right)MO \rightarrow CO_x + H_2O + \left(\frac{S_{CO} + 2S_{CO_2}}{S_{CO} + S_{CO_2}}\right)M, \tag{2S}$$

$$2M + O_2 \rightarrow 2MO. \tag{3S}$$

In these equations, MO represents an oxidized surface site and M a reduced surface site. The factor n_S is the moles of O_2 consumed per mole of CH_4 consumed. Oxidized and reduced active sites are taken to be the only surface species present and are thus conserved according to

$$\theta_{ox} + \theta_{red} = 1. \tag{10}$$

In Eq. (10), θ_{ox} is the fraction of active sites in the oxidized form (MO) and θ_{red} is the fraction of active sites in the reduced form (M).

The rates of reactions (1S) and (2S) are written as

$$r_{1S} = k_{1S} p_{CH_4} \theta_{ox}^2, \tag{11}$$

$$r_{3S} = k_{3S} p_{O_2} \theta_{red}^2 = k_{3S} p_{O_2} (1 - \theta_{ox})^2, \tag{12}$$

where r_{iS} is the reaction rate of reaction i on the SiO_2 surface, k_i is the corresponding rate constant, and p_j is the partial pressure of component j. We determined the fraction of the surface sites oxidized under given conditions θ_{ox} by equating the rates of surface reduction and oxidation at steady state:

$$n_S r_{1S} = r_{3S}. \tag{13}$$

The rate laws in Eqs. (11) and (12) are substituted into Eq. (13) and solved for θ_{ox} in terms of rate constants, partial pressures of CH_4 and O_2, and n_S. According to this kinetic scheme, θ_{ox} depends only on the ratio of partial pressures of CH_4 and O_2 [10].

If it is assumed that CO and CO_2 are formed exclusively by the reactions

$$CH_2O + MO \rightarrow CO + H_2O + M,$$

$$CH_2O + 2MO \rightarrow CO_2 + H_2O + 2M,$$

then n_S is related to the product distribution by

$$n_S = S_{CH_2O} + 1.5S_{CO} + 2S_{CO_2}. \tag{14}$$

Therefore, n_S is 1 for a product distribution of 100% CH_2O and 1.5 for 100% CO. Arena et al. demonstrated that θ_{ox} is insensitive to n_S and used $n_S = 1.25$, based on an approximate product distribution of 50% CH_2O, 50% CO. We observed a value of $n_S \approx 1.18$ for CH_4 oxidation over SiO_2 for the range of CH_4 conversions over which rate data were fit. However, as discussed below, the reaction of CH_2O over SiO_2 does not appear to consume oxygen, and hence we took $n_S = 1$ in Eq. (13).

Rate data for the oxidation of CH_4 over bare SiO_2 at 873 K are shown in Fig. 6. We increased the CH_4/O_2 feed ratio from 1.6 to 7.5 by increasing the feed fraction of CH_4 from 19 to 87% while holding the O_2 feed fraction constant at 13% (the balance was He). We further increased the CH_4/O_2 feed ratio to 22.7 by decreasing the O_2 feed fraction. The CH_4 oxidation rate exhibits a maximum at $CH_4/O_2 = 7.5$, where both reactants are at their maximum values. The model represented by Eqs. (10)–(13) was fit to the data by adjustment of the values of k_{1S}

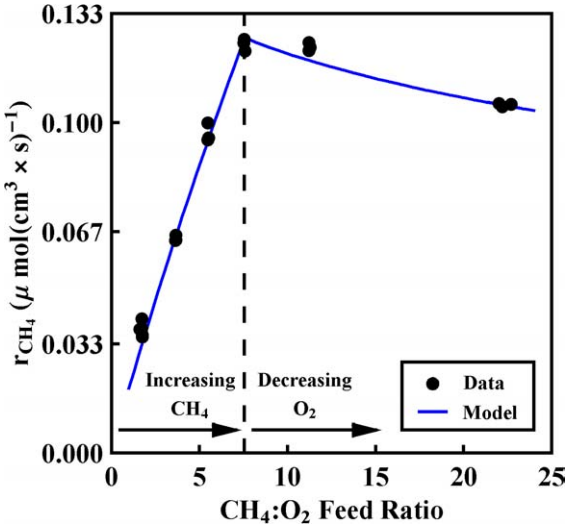

Fig. 6. Rate of CH_4 oxidation versus CH_4:O_2 ratio over bare SiO_2. CH_4 feed fraction was increased from 19 to 87% at 13% O_2 (balance He). CH_4 feed fraction was then held constant at 87% while O_2 feed fraction was reduced to 3.3% (balance He). Data recorded at 873 K with 0.65 s contact time. Model fit by varying k_{1S} and k_{3S}.

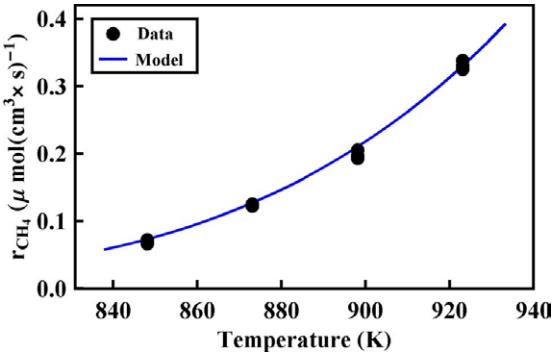

Fig. 7. Rate of CH_4 oxidation over bare SiO_2 versus temperature. Data recorded with 0.65 s contact time and feed composition of 87% CH_4, 13% O_2. Model fit by varying E_{1S} and E_{4S}.

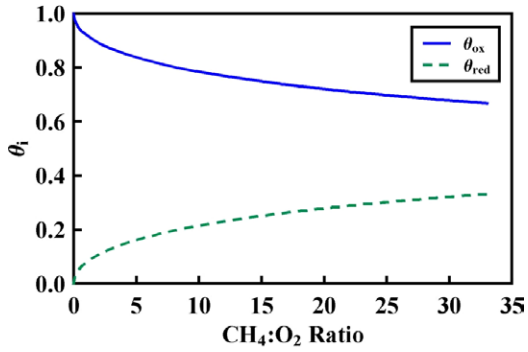

Fig. 8. SiO_2 surface state predicted by model versus CH_4:O_2 ratio at 923 K.

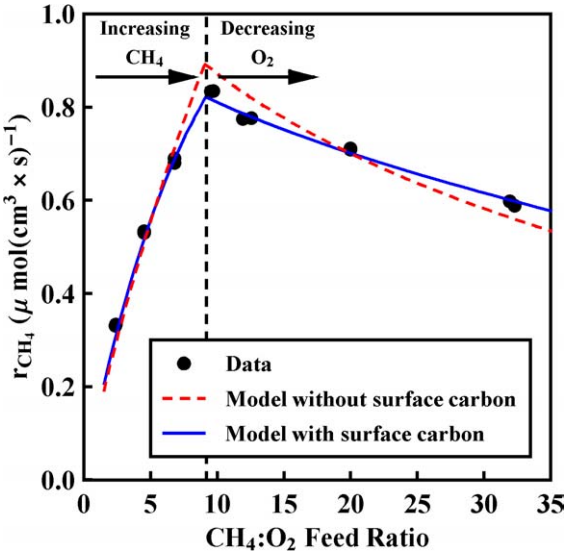

Fig. 9. Rate of CH_4 oxidation versus CH_4:O_2 ratio over MoO_x/SiO_2. CH_4 feed fraction was increased from 20 to 90% at 10% O_2 (balance He). CH_4 feed fraction was then held constant at 90% while O_2 feed fraction was reduced to 2.7% (balance He). Data recorded at 873 K at 0.85 s contact time. Dashed line shows model treating kinetics over MoO_x with rate laws of the same form as those used for bare SiO_2. Solid line shows model accounting for surface carbonaceous species.

and k_{4S}. As shown in Fig. 6, the model satisfactorily describes the CH_4 oxidation rate with respect to both reactants. Values of k_{1S} and k_{3S} at 873 K were found to be 0.122 and 50.3 μmol cm^{-3} atm^{-1} s^{-1}, respectively (0.466 and 192 nmol m^{-2} atm^{-1} s^{-1} when normalized by surface area). The ratio of the rate constants k_{1S}/k_{3S} is 0.0024, which is about 50% higher than the value of 0.00159 reported by Arena et al. [10] at 873 K. The temperature dependence of the CH_4 oxidation rate over bare SiO_2 is shown in Fig. 7. The two-site dissociative mechanism is fit to data with the assumption of Arrhenius forms for the rate constants k_{1S} and k_{3S}. A good fit to the data is obtained with values for the activation energies of $E_{1S} = 152$ kJ mol^{-1} and $E_{3S} = 0$. These values of E_{1S} and E_{3S} are in reasonable agreement with the findings of Arena et al., who reported activation energies of 159 and 20 kJ mol^{-1} for the respective reactions.

The speciation of the active sites on SiO_2 is plotted versus the CH_4/O_2 ratio at 923 K in Fig. 8. With the model formulated as described above, the speciation of active sites on the SiO_2 surface is completely specified by the CH_4/O_2 ratio. The fraction of oxidized sites predicted by the kinetic model falls from 88% at a CH_4/O_2 ratio of 2 to 67% at a CH_4/O_2 ratio of 33. Since the rate of CH_4 oxidation is proportional to the square of the fraction of oxidized sites, the rate of CH_4 oxidation decreases by 42%. The agreement between our model derived from kinetic observations and the pulse O_2 chemisorption observations of Arena et al. is quite good, but our model predicts a slightly more reduced surface over the range of CH_4/O_2 ratios for which data were available. At a CH_4/O_2 ratio of 8, our kinetic model predicts 20% surface vacancies, whereas O_2 chemisorption data reported by Arena et al. demonstrate 17% vacancies [10]. This small discrepancy could be ascribed to the different sources of SiO_2 in the two studies.

The rate of CH_4 oxidation over MoO_x/SiO_2 at 873 K is plotted versus the CH_4/O_2 ratio in Fig. 9. The exper-

imental conditions are the same as those employed in the experiments conducted over bare SiO_2 shown in Fig. 6. The CH_4 feed fraction is increased to raise the CH_4/O_2 feed ratio from 2 to 9, and we further raised the feed ratio by decreasing the O_2 feed fraction. The dashed line shows the best fit to the CH_4 oxidation rate data of a model formulated with the assumption that the rate laws for the reactions occurring on the supported MoO_x are of exactly the same form as those occurring on the SiO_2 surface (Eqs. (10)–(13)). It is evident that the two-site dissociative mechanism describing the SiO_2 surface is incapable of properly describing the kinetics occurring on the supported MoO_x. Although the general shape of the rate dependence is correct, the sensitivity of the rate to both the CH_4 and the O_2 partial pressures is too high.

To correctly model the kinetics occurring over the SiO_2-supported MoO_x, the mechanism assumed for SiO_2 must be modified to include another kinetically relevant surface species. This can be done by assuming that CH_2O is formed in a two-step process. The CH_4 is assumed to adsorb dissociatively and reversibly to yield methoxide species, which are then oxidized to yield CH_2O:

$$CH_4 + MO \rightleftarrows MOCH_3 + H_S, \tag{0M}$$

$$MOCH_3 + MO \rightarrow CH_2O + M + MOH. \tag{1M}$$

The oxidation of CH_2O over supported MoO_x and the reoxidation of MoO_x sites are assumed to occur via the following reactions:

$$CH_2O + \left(\frac{S_{CO} + 2S_{CO_2}}{S_{CO} + S_{CO_2}}\right)MO \rightarrow CO_x + H_2O + \left(\frac{S_{CO} + 2S_{CO_2}}{S_{CO} + S_{CO_2}}\right)M, \tag{2M}$$

$$2M + O_2 \rightarrow 2MO. \tag{3M}$$

The factor n_M is the ratio of the moles of O_2 consumed per mole of CH_4 consumed on the supported MoO_x moieties. The hydrogen atom formed in reaction (0M) is assumed to be bonded to the oxygen of a cleaved Mo–O–Si bond. This surface hydrogen is assumed to react rapidly with MOH formed from the oxidation of surface methoxide in reaction (1M) to release H_2O:

$$H_S + MOH \rightarrow H_2O + M. \tag{4M}$$

The surface-catalyzed oxidation of CH_4 to CH_2O and H_2O requires a four-electron reduction of the catalyst. Although the MoO_x sites of MoO_x/SiO_2 appear to be isolated as discussed above, the mechanism is written to include two molybdenum centers because MoO_x undergoes a two-electron reduction from Mo^{VI} to Mo^{IV} under reducing conditions at temperatures relevant to CH_4 oxidation [26], and hence two MoO_x centers are required to accommodate the oxidation of CH_4 to CH_2O. While spectroscopic observations indicate that the MoO_x moieties do not share bridging oxo groups, these species remain in relatively close proximity after their formation from polymolybdate species. The so-called microspreading of the polymolybdate present on the hydrated catalyst precursor to yield isolated MoO_x is believed to be a short-range phenomenon [23]. It has been demonstrated that MoO_3 does not spread over macroscopic distances on SiO_2 [38] and that polymolybdate is regenerated upon exposure of isolated MoO_x/SiO_2 to hydrating conditions [22], suggesting a close proximity of isolated MoO_x moieties. Methoxide was chosen as the most reasonable intermediate because it has been observed upon adsorption of CH_4 at low temperatures over MoO_x/SiO_2 by IR spectroscopy [39].

The rate laws for the reactions occurring on supported MoO_x are written as

$$r_{0M} = k_{0Mf} p_{CH_4} \phi_{ox} - k_{0Mr} \phi_C^2, \tag{15}$$

$$r_{1M} = k_{1M} \phi_C \phi_{ox}, \tag{16}$$

$$r_{3M} = k_{3M} p_{O_2} \phi_{red}^2, \tag{17}$$

where ϕ_{ox}, ϕ_C, and ϕ_{red} are the fractions of MoO_x present as oxidized sites (MO), sites with adsorbed methoxide ($MOCH_3$), and vacant sites (M), respectively. The subscripts f and r in Eq. (15) denote the forward and reverse rate constants for the dissociative adsorption of CH_4. The second-order dependence of the reverse reaction on ϕ_C arises because the amount of surface hydrogen H_S is approximately equal to the amount of $MOCH_3$. Surface hydrogen is formed and consumed by adsorption and desorption of CH_4 at the same rates as $MOCH_3$. Assuming that reaction (4M) occurs rapidly, then as soon as MOH is formed by oxidation of methoxide, surface hydrogen is consumed to yield H_2O. Hence, the amount of surface hydrogen is approximately equal to the amount of methoxide, and the reverse rate of the dissociative adsorption is described as an elementary process that is second-order in ϕ_C^2 (see Eq. (15)).

To solve for ϕ_{ox}, ϕ_{red}, and ϕ_C, it is necessary to write three steady-state balances for surface species. Balances on MO, $MOCH_3$, and total sites provide the necessary equations:

$$2r_{3M} - r_{0Mf} + r_{0Mr} - (n_M - 1)r_{1M} - (n_S - 1)\zeta r_{1S} = 0, \tag{18}$$

$$r_{0Mf} - r_{0Mr} - r_{1M} = 0, \tag{19}$$

$$\phi_{ox} + \phi_{red} + \phi_C = 1. \tag{20}$$

The quantity $-(n_S - 1)\zeta r_{1S}$ is included in the balance on MO (Eq. (18)) because H_2 resulting from non-oxidative decomposition of CH_2O over the SiO_2 surface is oxidized to H_2O by MO (see below). Here n_S is calculated from the observed product distribution during CH_4 oxidation over bare SiO_2 (rather than using $n_S = 1$ as in Eq. (13)), and n_M is approximated from the observed product distribution during CH_4 oxidation over MoO_x/SiO_2, in the same way as n_S is in Eq. (14). Although n_M is not strictly specified as n_S is in Eq. (14), since it accounts only for the reactions occurring over the supported MoO_x, Eq. (14) provides a good approximation of n_M because the majority of CH_4 oxidation occurs on supported MoO_x and the product distributions over SiO_2 and MoO_x/SiO_2 are similar. The values of n_S and n_M are not

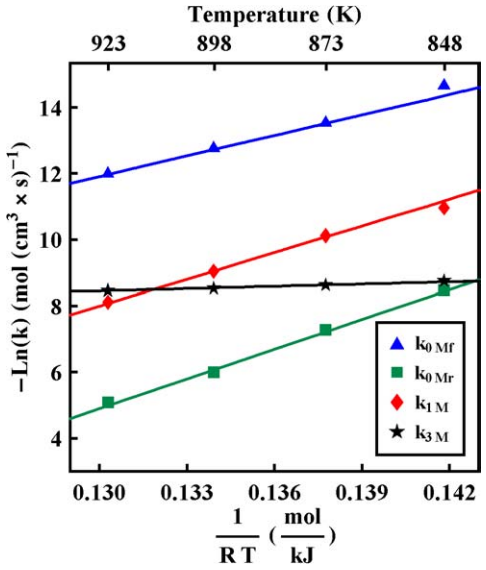

Fig. 10. Arrhenius plots of rate constants k_{0Mf}, k_{0Mr}, k_{1M}, and k_{3M} describing CH_4 oxidation over supported MoO_x. Data recorded with feed composition of 90% CH_4, 10% O_2 at 0.38 or 0.24 s contact time.

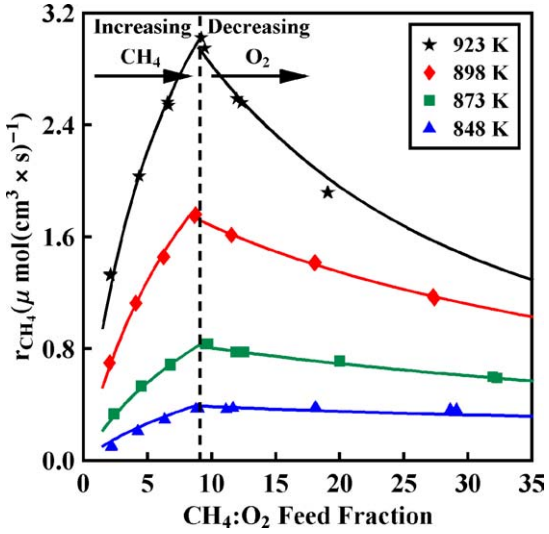

Fig. 11. Rate of CH_4 oxidation versus CH_4:O_2 ratio at temperatures of 848, 873, 898, and 923 K. Symbols are data; lines are model predictions using kinetic parameters extracted in Fig. 10. CH_4 feed fraction was increased from 20 to 90% at 10% O_2 (balance He). CH_4 feed fraction was then held constant at 90% while O_2 feed fraction was reduced to 3.3% (balance He). Data recorded at 0.38 s contact time at 848 and 873 K, and at 0.24 s contact time at 898 and 923 K.

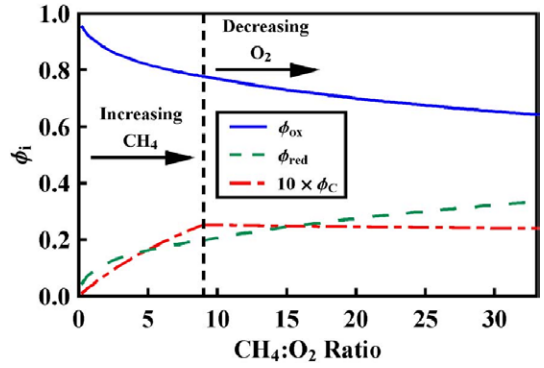

Fig. 12. Model predictions of MoO_x site speciation versus CH_4:O_2 ratio during CH_4 oxidation at 873 K. CH_4 feed fraction increased from 0 to 90% while holding O_2 feed fraction constant at 10%, then O_2 feed fraction decreased from 10 to 2.5% while holding CH_4 feed fraction constant at 90% (balance He). Percentage of surface carbonaceous species amplified 10 times.

constant over the length of the reactor but are taken as constants because they vary only slightly and the kinetic model is insensitive to their values. For the small conversion levels at which these expressions were fit to experimental data, the values of n_S and n_M were taken as 1.18 and 1.24, respectively.

From a fit of the model to the data shown in Fig. 9, the values of the rate constants k_{0Mf}, k_{0Mr}, k_{1M}, and k_{3M} at 873 K were determined to be 1.35 μmol cm^{-3} atm^{-1} s^{-1}, 710 μmol cm^{-3} s^{-1}, 40.6 μmol cm^{-3} s^{-1}, and 178 μmol cm^{-3} atm^{-1} s^{-1}, respectively. In order to calculate activation energies, we collected data similar to those shown in Fig. 9 at 848, 898, and 923 K. Values of the four rate constants were determined for each temperature; the values obtained are plotted in Fig. 10. Good linearity is observed for temperatures greater than 848 K. At 848 K the rates of reaction are relatively low, and the model begins to deviate from observations. The activation energies for the forward and reverse dissociative adsorption of CH_4, E_{0Mf} and E_{0Mr}, were found to be 206 and 299 kJ mol^{-1}, respectively, indicating an enthalpy loss of 93 kJ mol^{-1} upon dissociative adsorption of CH_4. The activation energy for oxidation of the surface methoxide species was found to be 269 kJ mol^{-1}. The rate of surface re-oxidation was practically unaffected by changes in temperature, and correspondingly E_{3M} is only 22.2 kJ mol^{-1}.

The fit of the model to the data is shown in Fig. 11 for temperatures between 848 and 923 K. The sensitivity of the rate of CH_4 oxidation to decreased oxygen partial pressure at high CH_4/O_2 ratios becomes greater at higher temperature. This is due in part to the greater decrease in O_2 partial pressure along the length of the reactor at higher rates, but is also due to the non-activated nature of the surface re-oxidation (reaction (3M)). The relatively large activation energies for the reactions of CH_4 cause the rates of surface reduction to increase sharply with temperature, whereas the rate of surface re-oxidation does not increase appreciably with temperature. As a result, more surface vacancies are present at higher temperature for a given gas-phase composition. The speciation of MoO_x sites predicted by the kinetic model is shown in Fig. 12 versus gas composition at 873 K. Increasing the gas-phase fraction of CH_4 from 20 to 90% at 10% O_2 increases the fraction of MoO_x with oxygen vacancies from 12 to 20% and increases the fraction of MoO_x with adsorbed methoxide from 0.8 to 2.5%. Decreasing the gas-phase O_2 fraction from 10 to 2.5% at 90% CH_4 results in a further increase of the fraction of vacancies to 34%. The fraction of MoO_x containing adsorbed methoxide species

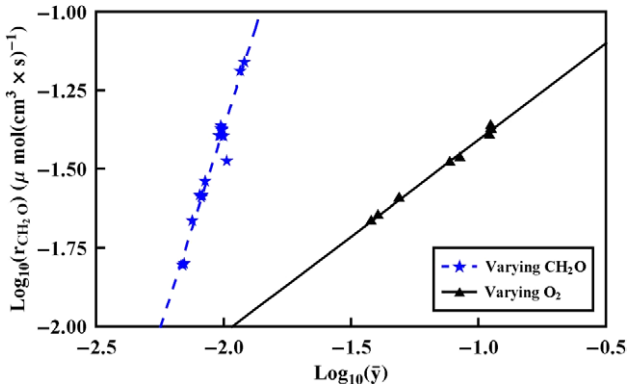

Fig. 13. Extraction of kinetic orders α and β of the homogeneous CH_2O reaction. (⋆) varying CH_2O at 11% O_2 feed fraction and (- - -) linear fit with slope of 2.55; (▲) varying O_2 feed fraction at 1.1% CH_2O feed fraction and (—) linear fit with slope of 0.61. Conversion of CH_2O was less than 20% throughout; conversion of O_2 was less than 2%. Recorded at 873 K, 1.62 atm absolute total pressure, and 0.9 s residence time.

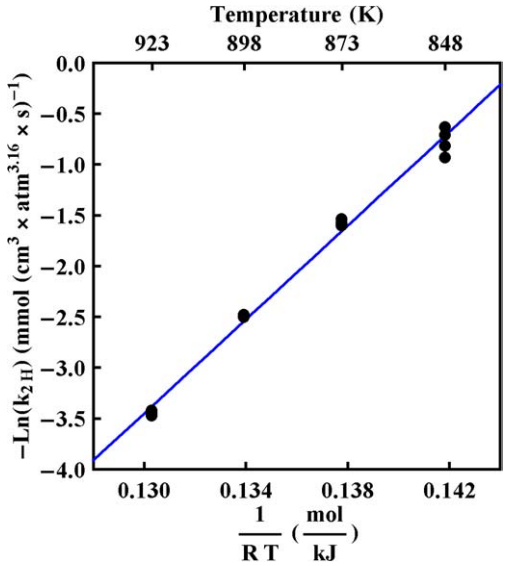

Fig. 14. Arrhenius plot of homogeneous CH_2O reaction rate. Feed composed of 1.1% CH_2O, 11% O_2, balance He at 1.62 atm absolute total pressure, 0.9 s residence time.

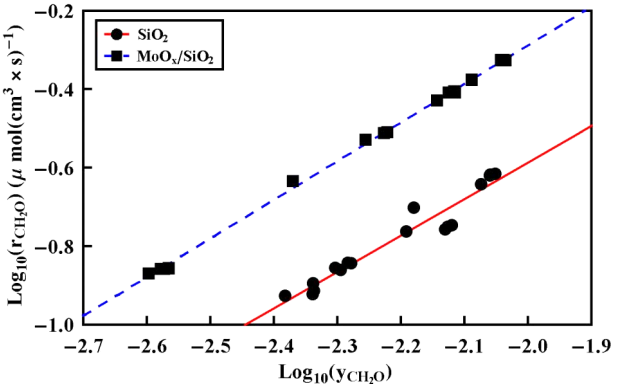

Fig. 15. Extraction of kinetic orders of CH_2O reaction with respect to CH_2O over bare SiO_2 and MoO_x/SiO_2. Varying CH_2O feed fraction at 11% O_2, balance He at 873 K. (●) Data recorded over bare SiO_2 and (—) linear fit with slope of 0.93; (■) data recorded over MoO_x/SiO_2 and (- - -) linear fit with slope of 0.98.

decreases slightly to 2.4%, as fewer oxidized sites are available for dissociative adsorption of CH_4. Thus, the fraction of MoO_x sites available for CH_4 oxidation (oxidized sites) decreases with increasing CH_4 partial pressure or decreasing O_2 partial pressure. This is manifested in the observed negative curvature of the CH_4 oxidation rate with increased CH_4 feed fraction and in the decreased CH_4 oxidation rate with decreased O_2 feed fraction.

4.4. Reactions of formaldehyde

The reaction of CH_2O over bare silica or supported MoO_x/SiO_2 has not received nearly the attention dedicated to the oxidation of CH_4 over the same catalysts, and hence the rate laws for the reaction of CH_2O are not as well known as those for CH_4 oxidation. Useful information regarding the rate laws was obtained from reaction of CH_2O/O_2/He mixtures over these catalysts at temperatures relevant to CH_4 oxidation. The homogeneous reaction of CH_2O was also investigated under the same reaction conditions to determine its relative importance during oxidation over the solid catalysts.

The homogeneous reaction of CH_2O produces CO_x, typically with a carbon selectivity of $>$ 90% CO and $<$ 10% CO_2. The homogeneous reaction proceeds via a radical network [8] and was modeled by a fit of rate data to an empirical rate law:

$$r_{2H} = k_{2H} p_{CH_2O}^{\alpha} p_{O_2}^{\beta}. \quad (21)$$

Fig. 13 shows rate data for homogeneous CH_2O reaction versus the mean CH_2O and O_2 molar fractions. The kinetic orders were extracted from the log–log plot shown rather than by use of a PFR model because the data showed good linearity on the log–log plot, and the additional precision afforded by the PFR model was deemed unnecessary. The data are well represented by Eq. (21) with $\alpha = 2.55$, $\beta = 0.61$, and $k_{2H} = 5.2 \times 10^{-3}$ mol cm^{-3} atm$^{-3.16}$ s^{-1}.

The large value of α is consistent with the observation of increased CH_2O conversion with increased CH_2O partial pressure made by Baldwin et al. [9]. The large exponent is attributable to the multiple roles of CH_2O and its fragments in the CH_2O reaction network. An Arrhenius plot of k_{2H} versus temperature for temperatures of 848 K to 923 K is shown as Fig. 14. The activation energy determined from the slope of this plot is 231 kJ mol^{-1}. This is higher than the values of 96 to 109 kJ mol^{-1} reported by other workers at temperatures of 573 to 823 K, but is comparable to the value of 209 kJ mol^{-1} reported for reaction vessels coated with "oxidation inhibitors" to suppress reactions occurring on the vessel walls [8].

Fig. 15 shows the dependence of the rate of CH_2O consumption at 873 K on the CH_2O feed fraction for reaction over bare SiO_2 and over MoO_x/SiO_2. The reaction obeys

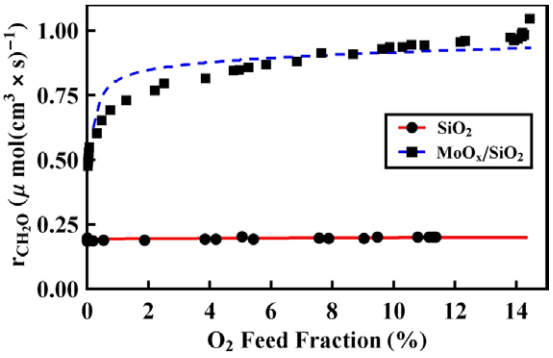

Fig. 16. Rate of CH_2O consumption versus O_2 feed fraction at 873 K with 1.1% CH_2O feed fraction. (•) Data recorded over bare SiO_2 and (—) model fit by varying k_{2S}; (■) data recorded over MoO_x/SiO_2 and (- - -) model fit by varying $k_{2M}^{(0)}$ and $k_{2M}^{(1)}$.

Table 2
Mean rates of CH_2O reaction at 873 K with 1.1% CH_2O feed fraction

Catalyst	r_{CH_2O} (μmol cm^{-3} s^{-1})	
	11% O_2	No O_2
Empty tube	0.043	0.005
SiO_2	0.20	0.19
MoO_x/SiO_2	0.95	0.49

first-order kinetics with respect to CH_2O over both SiO_2 and MoO_x/SiO_2, so linear regression of log–log data of the CH_2O consumption rate versus CH_2O feed fraction yields a slope of very nearly 1 in both cases.

The rate of CH_2O consumption at 873 K over bare SiO_2 and over MoO_x/SiO_2 is shown in Fig. 16 as a function of the fraction of O_2 in the feed. With no O_2 in the feed, CO and H_2 are produced in equivalent quantities, consistent with the pyrolytic decomposition of CH_2O:

$$CH_2O \rightarrow CO + H_2.$$

When bare SiO_2 is used as the catalyst, the rate of CH_2O consumption increases very slightly with increasing O_2 feed fraction, and only a small fraction (∼ 20%) of the H_2 generated is oxidized. The decomposition of CH_2O also occurs over the MoO_x moieties, as indicated by the increase in the rate of CH_2O decomposition in the absence of O_2 over MoO_x/SiO_2 (0.49 μmol cm^{-3} s^{-1} relative to the rate over bare SiO_2 (0.19 μmol cm^{-3} s^{-1}). As O_2 is added to the feed, the rate of CH_2O consumption over MoO_x/SiO_2 increases by almost a factor of 2 to 0.95 μmol cm^{-3} s^{-1}, and all H_2 formed is combusted to H_2O. In separate experiments in which H_2/O_2 mixtures were fed to the reactor, it was confirmed that the rate of H_2 combustion was very small over bare SiO_2 but comparable to the rate of reaction of CH_2O over MoO_x/SiO_2.

The mean reaction rates observed at the highest (11%) and lowest (0%) O_2 feed fractions studied are summarized in Table 2. The homogeneous reaction of CH_2O proceeds much more slowly than the reaction in the presence of either solid catalyst.

The rate laws utilized by Arena et al. [11] and Amiridis et al. [13] to describe CH_2O consumption during CH_4 oxidation over SiO_2 and MoO_x/SiO_2, respectively, assume that the reaction is oxidative and requires one surface oxygen to proceed (see reactions (2S) and (2M) above). Such rate laws will work as long as the fraction of oxidized surface sites does not vary greatly from the value for the reaction conditions under which the rate constant was determined. However, these rate laws will fail when the distribution of surface species deviates significantly because of changes in coverage by carbonaceous species or oxygen vacancies. A more physically meaningful model for the rate of CH_2O consumption can be constructed with the incorporation of terms into the rate expressions for CH_2O consumption accounting for the non-oxidative decomposition of CH_2O to CO. The following rate laws are therefore proposed to describe the reaction rates of CH_2O over bare SiO_2 and MoO_x/SiO_2, respectively:

$$r_{2S} = k_{2S} p_{CH_2O}, \tag{22}$$

$$r_{2M} = k_{2M}^{(0)} p_{CH_2O} \phi_{red} + k_{2M}^{(1)} p_{CH_2O} \phi_{ox}. \tag{23}$$

The rate law for CH_2O decomposition over SiO_2 is taken to be independent of the speciation of the active sites on SiO_2, consistent with the observed insensitivity of the reaction rate of CH_2O to the O_2 partial pressure over bare SiO_2. The (0) and (1) superscripts on k_{2M} in Eq. (23) refer to the rate constants for CH_2O decomposition and oxidation, respectively, on the supported MoO_x domains. The terms are assumed to represent, respectively, the activities of the reduced (M) sites and oxidized (MO) sites of the supported MoO_x as presented in the CH_4 oxidation model above.

The rate law for CH_2O decomposition over SiO_2 (Eq. (22)) was fit to the rate data for CH_2O over bare SiO_2 at 873 K shown in Fig. 16 by adjustment of the rate constant k_{2S}. The rate law for CH_2O reaction over the supported MoO_x moieties (Eq. (23)) was then fit to the corresponding rate data obtained over MoO_x/SiO_2 by adjustment of $k_{2M}^{(0)}$ and $k_{2M}^{(1)}$. A surface oxygen balance similar to Eq. (18) was utilized to track the fraction of oxygen vacancies on the supported MoO_x. The balance was constructed by equating the rate of MoO_x reduction by CH_2O and by the H_2 produced from non-oxidative CH_2O decomposition to the rate of surface re-oxidation already specified by the fit of CH_4 oxidation data:

$$2r_{3M} - r_{2M} - \zeta r_{2S} = 0. \tag{24}$$

It was assumed that no carbonaceous species are present on MoO_x sites during CH_2O oxidation because CH_2O is weakly adsorbed on oxides [13,40,41]. Eq. (24) is used together with the site conservation statement given by Eq. (20), taking $\phi_C = 0$. A similar balance is not necessary for the SiO_2, since the decomposition of CH_2O over SiO_2 is independent of the fraction of sites oxidized on SiO_2. The predictions of the model take into account contributions due to homogeneous reactions and reactions occurring on exposed

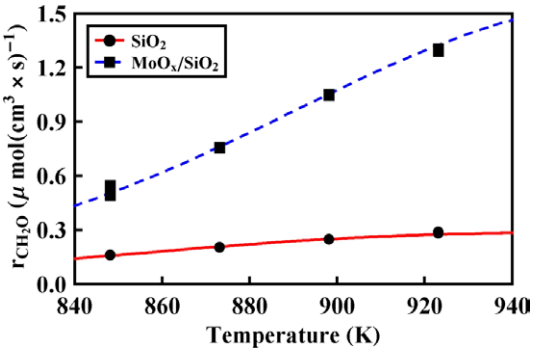

Fig. 17. Rate of CH_2O reaction versus temperature for reaction of CH_2O over (●) bare SiO_2 and (—) model fit by varying E_{2S}; (■) MoO_x/SiO_2 and (- - -) model fit by varying $E_{2M}^{(0)}$ and $E_{2M}^{(1)}$. Feed composition was 1.1% CH_2O, 11.5% O_2 (balance He).

SiO_2 and MoO_x, as described by Eqs. (5) and (6). The resulting fits of the model are shown with the rate data in Fig. 16. The best fits were obtained with rate constants of $k_{2S} = 18.3\ \mu mol\ cm^{-3}\ s^{-1}$, $k_{2M}^{(0)} = 7.91\ \mu mol\ cm^{-3}\ atm^{-1}\ s^{-1}$, and $k_{2M}^{(1)} = 24.5\ \mu mol\ cm^{-3}\ atm^{-1}\ s^{-1}$.

The O_2 dependence of the homogeneous reaction of CH_2O appears to account for the very slight increase in the rate of CH_2O consumption as the O_2 feed fraction is increased over bare SiO_2. The dependence of the CH_2O reaction rate over MoO_x/SiO_2 with respect to O_2 feed fraction is captured by the model, but the rate rises too sharply with O_2 feed fraction before reaching a plateau. This deviation is the result of a similar trend in fractional oxygen coverage, which rises very sharply with O_2 feed fraction at small O_2 feed fractions because the rate constant k_{3M} is large relative to the rate constants $k_{2M}^{(0)}$ and $k_{2M}^{(1)}$. Although the fit is not exact, the rate derived from the model deviates by less than 10% on a relative basis over the range of O_2 feed fractions studied. Furthermore, the fit obtained from Eq. (23) is not worse at any O_2 feed fraction than a fit obtained with the use of a rate law that does not include a non-oxidative component and provides a better fit at very small O_2/CH_2O ratios where surface oxygen vacancies become significant. As demonstrated in Fig. 12, the fraction of surface vacancies can be quite significant and can vary significantly with gas composition and temperature during CH_4 oxidation.

The temperature dependence of the CH_2O consumption rate over SiO_2 and over supported MoO_x was modeled with the assumption that the rate constants k_{2S}, $k_{2M}^{(0)}$, and $k_{2M}^{(1)}$ obey Arrhenius expressions, in which the corresponding activation energies are E_{2S}, $E_{2M}^{(0)}$, and $E_{2M}^{(1)}$. E_{2S} was fit to rate data obtained over bare SiO_2 at various temperatures, and then $E_{2M}^{(0)}$ and $E_{2M}^{(1)}$ were fit to similar data obtained over MoO_x/SiO_2. The resulting fits of the model to the experimental data are shown in Fig. 17. The activation energies used in the model are $E_{2S} = 109\ kJ\ mol^{-1}$, $E_{2M}^{(0)} = 125\ kJ\ mol^{-1}$, and $E_{2M}^{(1)} = 120\ kJ\ mol^{-1}$. The rate data appear to be well described by Eqs. (22) and (23).

The observations made here allow us to challenge two assertions made in the literature concerning CH_2O reaction at temperatures relevant to CH_4 oxidation. The first is that the reaction of CH_2O with O_2 proceeds over SiO_2 by a heterogeneous–homogeneous reaction mechanism, in which the SiO_2 surface initiates the formation of free radicals that decompose CH_2O in the gas phase [6]. This assertion was based on the observation by mass spectrometry of $HO_2\cdot$ radicals at a number density of about $10^{13}\ cm^{-3}$ during the oxidation of CH_2O over bare SiO_2 at 873 K. Inserting this concentration of $HO_2\cdot$ into the rate law reported by Eiteneer et al. [42] for the decomposition of CH_2O by $HO_2\cdot$, we estimate the rate of CH_2O decomposition at 873 K and 1.5 atm for a feed containing 1% CH_2O to be 0.01 $\mu mol\ cm^{-3}\ s^{-1}$. This is about four orders of magnitude less than the rates observed over SiO_2 in the present study, which suggests that the $HO_2\cdot$ observed by Nersessian et al. is kinetically irrelevant. It can similarly be demonstrated with the use of combustion kinetic data [43] that the concentration of $H\cdot$ necessary to produce the observed concentration of $HO_2\cdot$ is much too small to decompose CH_2O at the observed reaction rate. These conclusions are supported by our observations of the change in the order of reaction with respect to CH_2O from 2.55 to 1.0 as we go from homogeneous CH_2O oxidation to heterogeneous CH_2O oxidation over SiO_2. The reduction in the reaction order in the presence of SiO_2 may be caused by quenching of the radical mechanism by radical recombination on the SiO_2 surface [9] or simply by the first-order heterogeneous reaction proceeding at a much greater rate than the higher-order homogeneous reaction.

Bañares and Fierro have also claimed that the reaction of CH_2O over MoO_x/SiO_2 proceeds primarily in the gas phase based on their observations regarding the deleterious effects of a heated post-reactor volume on the CH_2O selectivity during CH_4 oxidation [7]. While homogeneous reaction can indeed destroy an appreciable amount of CH_2O given sufficient contact time, the present investigation has shown that the void volume within the packed bed is insufficient for the homogeneous reaction to contribute appreciably to the consumption of CH_2O for the feed rates studied. Careful attention to reactor design, as described by Bañares and Fierro (exclusion of post-reactor volume and use of small-ID tubing to transport the products rapidly out of the heated zone), is important for minimization of the effects of the homogeneous reaction downstream of the catalyst bed, but within the catalyst the homogeneous component of the reaction appears to be insignificant.

4.5. Model analysis

The kinetic parameters and the rate laws describing the consumption of CH_4 and CH_2O are summarized in Table 3. This information can now be used to simulate the observed trends in CH_4 conversion and CH_2O selectivity versus contact time. To utilize the model in a predictive fashion, we cast the surface oxygen balances in terms of the rates of surface

Table 3
Summary of kinetic parameters

Rate constant	Kinetic group	Rate constant at 873 K			Pre-exponential factor, A_i	Activation energy, E_i
		k_i (873 K)	k_i' (873 K)	k_i'' (873 K)		
$CH_4 \rightarrow CH_2O$						
k_{1S}	$p_{CH_4}\theta_{ox}^2$	0.122 μmol cm^{-3} atm^{-1} s^{-1}	0.466 nmol m^{-2} atm^{-1} s^{-1}	–	145 mol cm^{-3} atm^{-1}s^{-1}	152 kJ mol^{-1}
k_{0Mf}	$p_{CH_4}\phi_{ox}$	1.35 μmol cm^{-3} atm^{-1} s^{-1}	–	6.44×10^{-3} mol mol$_{Mo}^{-1}$ atm^{-1}s^{-1}	2.86×10^{6} mol cm^{-3} atm^{-1} s^{-1}	206 kJ mol^{-1}
k_{0Mr}	$\phi_C\phi_H$	710 μmol cm^{-3} s^{-1}	–	3.39 mol mol$_{Mo}^{-1}$ s^{-1}	5.72×10^{14} mol cm^{-3} s^{-1}	299 kJ mol^{-1}
k_{1M}	$\phi_{ox}\phi_C$	40.6 μmol cm^{-3} s^{-1}	–	0.194 mol mol$_{Mo}^{-1}$ s^{-1}	4.77×10^{11} mol cm^{-3} s^{-1}	269 kJ mol^{-1}
$CH_2O \rightarrow CO_x$						
k_{2H}	$p_{CH_2O}^{2.65}p_{O_2}^{0.55}$	5.2×10^{-3} μmol cm^{-3} atm$^{-3.16}$ s^{-1}	–	–	3.54×10^{11} mol cm^{-3} atm$^{-3.16}$ s^{-1}	231 kJ mol^{-1}
k_{2S}	p_{CH_2O}	18.3 μmol cm^{-3} atm^{-1} s^{-1}	58.3 nmol m^{-2} atm^{-1} s^{-1}	–	57.3 mol cm^{-3} atm^{-1}s^{-1}	109 kJ mol^{-1}
$k_{2M}^{(0)}$	$p_{CH_2O}\phi_{red}$	7.91 μmol cm^{-3} atm^{-1}s^{-1}	–	0.0390 mol mol$_{Mo}^{-1}$ atm^{-1}s^{-1}	237 mol cm^{-3} atm^{-1}s^{-1}	125 kJ mol^{-1}
$k_{2M}^{(1)}$	$p_{CH_2O}\phi_{ox}$	24.5 μmol cm^{-3} atm^{-1}s^{-1}	–	0.117 mol mol$_{Mo}^{-1}$ atm^{-1}s^{-1}	1690 mol cm^{-3} atm^{-1}s^{-1}	131 kJ mol^{-1}
$M \rightarrow MO$						
k_{3S}	$p_{O_2}\theta_{red}^2$	50.3 μmol cm^{-3} atm^{-1}s^{-1}	192 nmol m^{-2} atm^{-1}s^{-1}	–	5.03×10^{-5} mol cm^{-3} atm^{-1} s^{-1}	0 kJ mol^{-1}
k_{3M}	$p_{O_2}\phi_{red}^2$	178 μmol cm^{-3} atm^{-1} s^{-1}	–	0.850 mol mol$_{Mo}^{-1}$ atm^{-1} s^{-1}	3.80×10^{-3} mol cm^{-3} atm^{-1} s^{-1}	22.2 kJ mol^{-1}

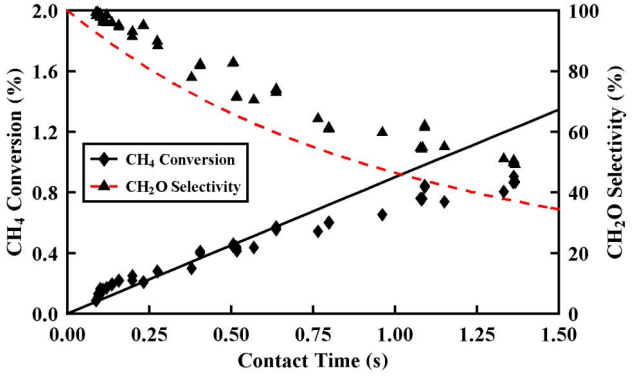

Fig. 18. CH_4 conversion and CH_2O selectivity during CH_4 oxidation over bare SiO_2 at 873 K with feed consisting of 90% CH_4, 10% O_2. (♦) Observed CH_4 conversion and (—) model prediction; (▲) observed CH_2O selectivity and (- - -) model prediction.

reduction and oxidation, rather than in terms of the parameter n_i. The balance on oxidized MoO_x sites (Eq. (18)) is re-written as

$$2r_{3M} - r_{0Mf} + r_{0Mr} - r_{1M} - \left(\frac{S_{CO} + 2S_{CO_2}}{S_{CO} + S_{CO_2}}\right) r_{2M} - \zeta r_{2S} = 0. \quad (25)$$

The CH_2O consumed by non-oxidative processes over both exposed SiO_2 and supported MoO_x is accounted for in the MoO_x oxygen balance because the H_2 produced by these processes is oxidized to H_2O over MoO_x. The bracketed term in Eq. (25) accounts for the additional surface oxygen consumed in the generation of CO_2. The product distribution during the oxidation of CH_2O over MoO_x/SiO_2 is typically 90% CO, 10% CO_2, so the bracketed term is approximated as 1.1. This is a good approximation because the term varies weakly with the product distribution (going from 1.1 at a CO/CO_2 ratio of 9 to 1.2 at a CO/CO_2 ratio of 6). At contact times shorter than the time of maximum CH_2O yield, this assumption is even more appropriate because the rate of CH_4 oxidation is faster than the rate of CH_2O consumption. For SiO_2, it was possible to continue using Eq. (13) with $n_S = 1$, since CH_2O decomposition does not consume surface oxygen.

Comparisons of the model predictions with experimental data observed during CH_4 oxidation over bare SiO_2 are shown in Fig. 18. Consumption of both CH_4 and CH_2O appears to occur somewhat more slowly over the bare SiO_2 than is predicted by the model. The predicted CH_4 conversion is about 33% higher than the observed rate at a contact time of 1.25 s, and the predicted CH_2O selectivity is about 33% lower than the observed selectivity. The model predictions are better at shorter times. The deviation may be due in part to experimental error and may also be related to the variation in H_2O partial pressure with contact time, as H_2O is unaccounted for in the model and may in fact inhibit CH_4 oxidation. Because the rate of CH_4 oxidation over SiO_2 is small relative to the corresponding rate over supported MoO_x, this deviation is not of great concern. It

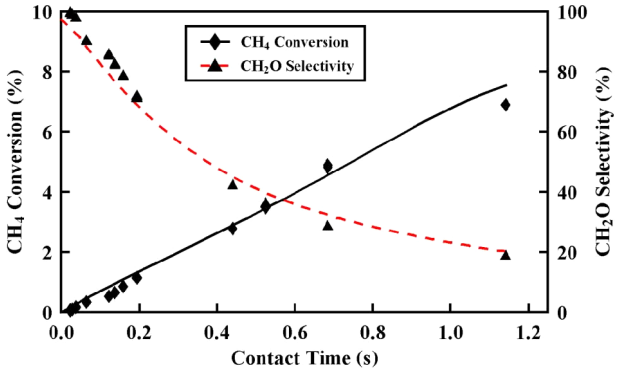

Fig. 19. CH_4 conversion and CH_2O selectivity during CH_4 oxidation over MoO_x/SiO_2 at 873 K with feed consisting of 90% CH_4, 10% O_2. (♦) Observed CH_4 conversion and (—) model prediction; (▲) observed CH_2O selectivity and (- - -) model prediction.

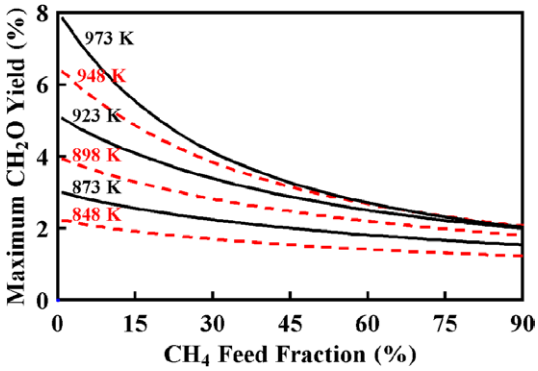

Fig. 20. Model predictions of maximum CH_2O yield with respect to contact time versus CH_4 feed fraction at various temperatures. O_2 feed fraction held constant at 10%, total pressure of 1.5 atm absolute.

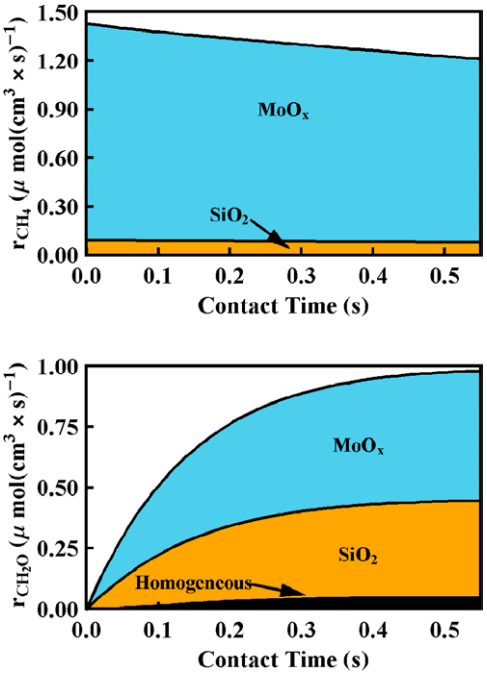

Fig. 21. Mean rates of CH_4 oxidation and CH_2O consumption in each of the reactive media versus contact time at 923 K, 1.5 atm during CH_4 oxidation with feed composed of 20% CH_4, 10% O_2 (balance He). The slope of the top curve in each plot is the total local rate. The maximum CH_2O yield occurs at 0.29 s under these conditions, where the total local rates of CH_4 oxidation and CH_2O consumption are equal.

should be noted that the predicted CH_2O selectivity versus CH_4 conversion is excellent, as the observed rate of CH_2O decomposition (as measured by the CH_2O selectivity) is slower by approximately the same factor as the observed rate of CH_4 oxidation.

The predicted trends for CH_4 oxidation over MoO_x/SiO_2 at 873 K with 90% CH_4, 10% O_2 are compared with the observed data in Fig. 19. The model predictions are in very good agreement with observations of both CH_4 conversion and CH_2O selectivity over the entire range of the data. Deviations are less than 10 relative % over the entire range.

Since the model provides a good description of CH_4 conversion and CH_2O selectivity for MoO_x/SiO_2 and was developed from observations made over a wide range of temperatures and gas-phase compositions, it can be used to assess the impact of reaction conditions on the CH_2O yield. Fig. 20 shows the effects of both feed composition and temperature on the maximum single-pass yield achievable with respect to contact time over MoO_x/SiO_2. The highest single-pass yields are possible when the rate of CH_4 oxidation is maximized relative to the rate of CH_2O consumption. The rate of CH_4 oxidation is more sensitive to the fraction of oxidized sites than is the rate of reaction of CH_2O. CH_4 oxidation is second-order in the fraction of oxidized sites over the exposed SiO_2 and pseudo-second-order in the fraction of oxidized sites over MoO_x, whereas reaction of CH_2O is independent of the fraction of oxidized sites over SiO_2 and first-order in the fraction of oxidized sites over MoO_x. Hence the maximum single-pass yield achievable increases with decreasing CH_4/O_2 ratio as the surface fractions of oxidized sites become greater. At 923 K, the maximum possible CH_2O yield increases from 2.0 to 5.1% as the CH_4 feed fraction is decreased from 90 to 1% while the O_2 feed fraction is held constant at 10%. Because the activation energies for CH_4 oxidation are large relative to the activation energies for CH_2O decomposition and oxidation, the rate of CH_4 oxidation increases faster than the rate of CH_2O consumption with increasing temperature, so the maximum possible yield increases with temperature. This effect is much more pronounced at small CH_4/O_2 ratios. High CH_4/O_2 ratios diminish the effect of increasing temperature, as the balance of surface sites is shifted away from oxidized sites under these conditions. With a feed composed of 1% CH_4, 10% O_2, the maximum CH_2O yield increases from 2.2% at 848 K to 7.8% at 973 K, but with a feed composed of 90% CH_4, 10% O_2, the maximum CH_2O yield only increases from 1.2 to 2.0%. This is consistent with the observations of Spencer and Pereira, who observed only a very slight increase in the profile of CH_2O selectivity versus CH_4 conversion with increasing temperature when they conducted experiments at a CH_4/O_2 ratio of 9 [14].

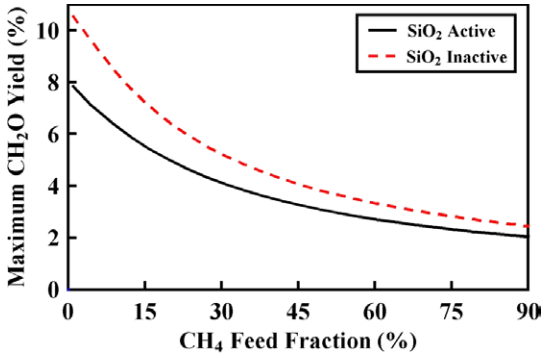

Fig. 22. Maximum CH_2O yield with respect to contact time versus CH_4:O_2 ratio for CH_4 oxidation at 973 K, 1.5 atm with 10% O_2 feed fraction over MoO_x/SiO_2. (—) All reaction pathways active (real system as modeled); (- - -) SiO_2 pathways inactive.

Having defined the contributions of the gas-phase, support, and supported MoO_x, it is possible to isolate the intrinsic activity of the supported MoO_x. Fig. 21 shows the contribution of each locus of reaction on the total rates of reaction during CH_4 oxidation at 923 K for a feed composed of 20% CH_4, 10% O_2. These contributions were determined by constructing the gas-phase and surface species profiles versus contact time, integrating the local rates of reaction in each of the reactive media over the length of the reactor, and normalizing by the total contact time. The observed rate of reaction is the sum over $\langle r_i \rangle$ for reaction occurring in the gas phase, on the exposed SiO_2, and on the supported MoO_x.

$$\langle r_i \rangle = \frac{1}{\tau} \int_0^{\tau} r_i(\tau')\, d\tau'. \tag{26}$$

The overall rate of reaction is given by the uppermost curve in Fig. 21. The rate of reaction at a given contact time within the reactor is proportional to the slope of the uppermost curve, and the maximum yield is obtained when the slopes of the CH_2O consumption rate and CH_4 oxidation rate are equal but opposite. This occurs at $\tau = 0.29$ s for the conditions shown in Fig. 21. At this contact time, the mean CH_4 oxidation rate over the supported MoO_x is 1.17 μmol cm^{-3} s^{-1}, whereas the mean rate of CH_4 oxidation over the exposed SiO_2 is only 0.082 μmol cm^{-3} s^{-1}. The mean rates of CH_2O consumption at this contact time are 0.483, 0.358, and 0.041 μmol cm^{-3} s^{-1} on the MoO_x, on the exposed SiO_2, and in the gas-phase, respectively. Hence the effect of the exposed SiO_2 on the observed activity is deleterious, as it contributes to the consumption of CH_2O to a greater extent than it does to the formation of CH_2O.

To determine the activity of MoO_x on a completely inert support, the rates of the reactions over SiO_2 are set to zero in the model. The resulting increase in the maximum CH_2O yield with respect to contact time is plotted in Fig. 22 versus the CH_4 feed fraction at 973 K while the O_2 feed fraction is held constant at 10%. When a completely inert support is used, the maximum CH_2O yield increases from 7.8 to 10.5% at 1% CH_4, or from 2.0 to 2.5% at 90% CH_4.

5. Conclusions

A model has been developed to describe the kinetics of the selective oxidation of methane to formaldehyde over MoO_x/SiO_2. This model accounts for the reactions of methane and formaldehyde occurring in the gas phase and on the surfaces of the silica support and the dispersed molybdena. The overall rate of reaction, predicted by the model as the sum of the rates of reaction proceeding in the gas phase and on the catalyst surface, very accurately describes the rate of CH_4 oxidation and the selectivity of the products for CH_2O observed experimentally. Since the kinetics of homogeneous reaction and heterogeneous reaction occurring on SiO_2 and MoO_x are each known, it is possible to use the model to assess the importance of each contribution to the overall performance of the catalyst.

The oxidation of CH_4 is found to proceed almost exclusively over the supported molybdena. The rate of homogeneous oxidation is negligible at the pressures used in this study, and the rate of CH_4 oxidation over bare SiO_2 is about an order of magnitude less than that over the supported MoO_x. Although the rate of gas-phase CH_2O oxidation is measurable, the void volume within the catalyst is insufficient for this process to make a significant contribution to overall rate of CH_2O consumption. The principal process occurring over bare SiO_2 is CH_2O decomposition to form CO and H_2. Even in the presence of excess O_2, very little of the H_2 undergoes combustion. CH_2O decomposition also occurs on the supported MoO_x. When O_2 is present in the feed, all of the H_2 formed from CH_2O decomposition is combusted on the supported MoO_x.

The maximum single-pass conversion of CH_4 to CH_2O is strongly influenced by temperature and CH_4/O_2 ratio in the feed. The maximum single-pass yield increases with increasing temperature and decreasing CH_4/O_2 ratio. For the catalyst studied a maximum CH_2O yield of 7.0% could be achieved at a temperature of 973 K with a feed composed of 5% CH_4 and 10% O_2 in He. A further gain of 2.5% could be achieved if the surface of SiO_2 were made completely inactive.

Acknowledgment

This work was supported by the Methane Conversion Cooperative sponsored by BP.

References

[1] T.H. Fleisch, R. Puri, R.A. Sills, A. Basu, M. Gradassi, G.R. Jones Jr., in: J.J. Spivey, E. Iglesia, T.H. Fleisch (Eds.), Natural Gas Conversion VI, in: Studies in Surface Science and Catalysis, vol. 136, Elsevier Science B.V., Amsterdam, 2001, p. 423.
[2] R. Pitchai, K. Klier, Catal. Rev.-Sci. Eng. 28 (1986) 13.
[3] K. Otsuka, Y. Wang, Appl. Catal. A 222 (2001) 145.
[4] A. Parmaliana, F. Arena, F. Frusteri, A. Martinez-Arias, M.L. Granados, J.L.G. Fierro, Appl. Catal. A 226 (2002) 163.

[5] W.-H. Cheng, J. Catal. 158 (1996) 477.
[6] L.A. Nersessian, A.A. Muradian, T.A. Gharibian, L.Y. Margolis, A.B. Nalbandian, Arm. Khim. 31 (1978) 33.
[7] M.A. Bañares, J.L.G. Fierro, in: T. Oyama, J.W. Hightower (Eds.), Catalytic Selective Oxidation, in: ACS Symposium Series, vol. 523, ACS, Washington, D.C., 1993, p. 354.
[8] J.F. Walker, Formaldehyde, third ed., ACS Monograph Series, Reinhold, New York, 1964, p. 210.
[9] T.R. Baldwin, R. Burch, G.D. Squire, S.C. Tsang, Appl. Catal. 74 (1991) 137.
[10] F. Arena, F. Frusteri, A. Parmaliana, AIChE J. 46 (11) (2000) 2285.
[11] F. Arena, F. Frusteri, A. Parmaliana, J. Catal. 207 (2002) 232.
[12] D. Miceli, F. Arena, A. Parmaliana, M.S. Scurrell, V. Sokolovskii, Catal. Lett. 18 (1993) 283.
[13] M.D. Amiridis, J.E. Rekoske, J.A. Dumesic, D.F. Rudd, N.D. Spencer, C.J. Pereira, AIChE J. 37 (1991) 87.
[14] N.D. Spencer, J. Catal. 109 (1988) 187.
[15] N.D. Spencer, C.J. Pereira, R.K. Graselli, J. Catal. 126 (1990) 546.
[16] G.F. Froment, K.B. Bischoff, Chemical Reactor Analysis and Design, second ed., Wiley, New York, 1990, p. 166.
[17] G.C. Bond, S. Flamerz, L.V. Wijk, Catal. Today 1 (1987) 229.
[18] F.L. Galeener, A.E. Geissberger, Phys. Rev. B 27 (10) (1983) 6199.
[19] J.C. Phillips, Phys. Rev. B 35 (12) (1987) 6409.
[20] F.L. Galeener, R.H. Geils, in: P.H. Gaskell (Ed.), The Structure of Non-Crystalline Materials, Taylor and Francis, London, 1977, p. 223.
[21] G. Mestl, T.K.K. Srinivasan, Catal. Rev.-Sci. Eng. 40 (4) (1998) 451.
[22] M.A. Bañares, I.E. Wachs, J. Raman Spectrosc. 33 (2002) 359.
[23] M. de Boer, A.J. van Dillen, D.C. Koningsberger, J.W. Geus, M.A. Vuurman, I.E. Wachs, Catal. Lett. 11 (1991) 227.
[24] M.A. Bañares, N.D. Spencer, M.D. Jones, I.E. Wachs, J. Catal. 146 (1994) 204.
[25] M.A. Bañares, H. Hu, I.E. Wachs, J. Catal. 150 (1994) 407.
[26] A.N. Desikan, L. Huang, S.T. Oyama, J. Phys. Chem. 95 (1991) 10050.
[27] Y. Iwasawa, Adv. Catal. 35 (1987) 187.
[28] M. Cornac, A. Janin, J.C. Lavalley, Polyhedron 5 (1–2) (1986) 183.
[29] C.C. Williams, J.G. Ekerdt, J. Phys. Chem. 95 (1991) 8781.
[30] G. Martra, P. Vittone, S. Coluccia, F. Arena, A. Parmaliana, Il Nuovo Cimento 19 (11) (1997) 1727.
[31] H. Hu, I.E. Wachs, S.R. Bare, J. Phys. Chem. 99 (1995) 10897.
[32] M. Fournier, C. Louis, M. Che, P. Chaquin, D. Masure, J. Catal. 119 (1989) 400.
[33] K. Chen, E. Iglesia, A.T. Bell, J. Phys. Chem. 104 (2000) 10059.
[34] M.A. Bañares, I. Rodriguez-Ramos, A. Guerrero-Ruiz, J.L.G. Fierro, in: L. Guczi (Ed.), New Frontiers in Catalysis, Proceedings of the 10th International Congress on Catalysis, in: Studies in Surface Science and Catalysis, vol. 75, Elsevier, Amsterdam, 1993, p. 1131.
[35] A. Parmaliana, V. Sokolovskii, D. Miceli, F. Arena, N. Giordano, J. Catal. 148 (1994) 514.
[36] F. Arena, F. Frusteri, A. Parmaliana, N. Giordano, Appl. Catal. 125 (1995) 39.
[37] N.D. Spencer, C.J. Pereira, AIChE J. 33 (1987) 1808.
[38] J. Leyrer, D. Mey, H. Knözinger, J. Catal. 124 (1990) 349.
[39] H.-F. Liu, R.-S. Liu, K.Y. Liew, R.E. Johnson, J.H. Lunsford, J. Am. Chem. Soc. 106 (1984) 4117.
[40] F.S. Feil, J.G. van Ommen, J.R.H. Ross, Langmuir 3 (1987) 668.
[41] G. Busca, J. Mol. Catal. 50 (1989) 241.
[42] B. Eiteneer, C.-L. Yu, M. Goldenberg, M. Frenklach, J. Phys. Chem. A 102 (1998) 5196.
[43] D.L. Baulch, C.J. Cobos, R.A. Cox, P. Frank, G. Hayman, Th. Just, J.A. Kerr, T. Murrells, M.J. Pilling, et al., J. Phys. Chem. Ref. Data 23 (6) (1994) 847.